Interpretation of Young's equation for a liquid droplet on a flat and smooth solid surface: Mechanical and thermodynamic routes with a simple Lennard-Jones liquid

Interpretation of Young's equation for a liquid droplet on a flat and smooth solid surface: Mechanical and thermodynamic routes with a simple Lennard-Jones liquid

Yasutaka Yamaguchi (iD), Hiroki Kusudo, Donatas Surblys (iD), Takeshi Omori (iD), and Gota Kikugawa (iD)

View Online   Export Citation   CrossMark

ARTICLES YOU MAY BE INTERESTED IN

Lock-in Amplifiers
... and more, from DC to 600 MHz   Watch

Interpretation of Young's equation for a liquid droplet on a flat and smooth solid surface: Mechanical and thermodynamic routes with a simple Lennard-Jones liquid

Yasutaka Yamaguchi,[1,2,a] Hiroki Kusudo,[1,b] Donatas Surblys,[3,c] Takeshi Omori,[1,d]
and Gota Kikugawa[3,e]

AFFILIATIONS

[1] Department of Mechanical Engineering, Osaka University, 2-1 Yamadaoka, Suita 565-0871, Japan
[2] Water Frontier Science and Technology Research Center (W-FST), Research Institute for Science and Technology, Tokyo University of Science, 1-3 Kagurazaka, Shinjuku-ku, Tokyo 162-8601, Japan
[3] Institute of Fluid Science, Tohoku University, 2-1-1 Katahira, Aoba-ku, Sendai 980-8577, Japan

[a] Electronic mail: yamaguchi@mech.eng.osaka-u.ac.jp. URL: http://www-gcom.mech.eng.osaka-u.ac.jp.
[b] Electronic mail: hiroki@gcom.mech.eng.osaka-u.ac.jp
[c] Electronic mail: donatas@microheat.ifs.tohoku.ac.jp
[d] Electronic mail: t.omori@mech.eng.osaka-u.ac.jp
[e] Electronic mail: kikugawa@microheat.ifs.tohoku.ac.jp

ABSTRACT

In this study, we carried out molecular dynamics simulations of a cylindrical Lennard-Jones droplet on a flat and smooth solid surface and showed that Young's equation as the relation among solid-liquid, solid-vapor, and liquid-vapor interfacial tensions γ_{SL}, γ_{SV}, and γ_{LV}, respectively, was applicable only under a very restricted condition. Using the fluid stress-tensor distribution, we examined the force balance in the surface-lateral direction exerted on a rectangular control volume set around the contact line. As the mechanical route, the fluid stress integrals along the two control surfaces normal to the solid-fluid interface were theoretically connected with γ_{SL} and γ_{SV} relative to the solid-vacuum interfacial tension γ_{S0} by Bakker's equation extended to solid-related interfaces via a thought experiment, for which the position of the solid-fluid interface plane was defined at the limit that the fluid molecules could reach. On the other hand, the fluid stress integral along the control surface lateral to the solid-fluid interface was connected with γ_{LV} by the Young-Laplace equation. Through this connection, we showed that Young's equation was valid for a system in which the net lateral force exerted on the fluid molecules from the solid surface was zero around the contact line. Furthermore, we compared $\gamma_{SL} - \gamma_{S0}$ and $\gamma_{SV} - \gamma_{S0}$ obtained by the mechanical route with the solid-liquid and solid-vapor works of adhesion obtained by the dry-surface method as one of the thermodynamic routes and showed that both routes resulted in a good agreement. In addition, the contact angle predicted by Young's equation with these interfacial tensions corresponded well to the apparent droplet contact angle determined by using the previously defined position of the solid-fluid interface plane; however, our theoretical derivation indicated that this correspondence was achieved because the zero-lateral force condition was satisfied in the present system with a flat and smooth solid surface. These results indicated that the contact angle should be predicted not only by the interfacial tensions but also by the pinning force exerted around the contact line.

I. INTRODUCTION

The behavior of the contact line, where a liquid-vapor interface meets a solid surface, has long been a topic of interest in various science and engineering fields because it plays a key role in the wetting properties.[1–3] By introducing the concept of interfacial tensions and contact angle θ, Young's equation[4] is given by

$$\gamma_{SL} - \gamma_{SV} + \gamma_{LV} \cos \theta = 0, \tag{1}$$

where γ_{SL}, γ_{SV}, and γ_{LV} denote solid-liquid, solid-vapor, and liquid-vapor interfacial tensions, respectively. The contact angle is a common measure of wettability at the macroscopic scale. Historically, Young's equation (1) was first proposed based on the horizontal force balance of interfacial tensions exerted on the contact line in 1805 before the establishment of thermodynamics.[5] Instead of using the concept of force balance, Young's equation is often re-defined from a thermodynamic point of view.[1] Various models have been further put forward to capture the details of the contact line, such as introducing microscopic contact angle,[6] adding line tension term to Eq. (1),[7,8] and dealing with precursor films.[1,9] However, it is difficult to experimentally validate these models mainly because measuring the interfacial tensions γ_{SL} and γ_{SV}, which include the solid phase, is not trivial.[10,11] It should also be noted that recent micro-structuring techniques can produce a heterogeneous solid surface with a well-defined boundary between areas having different wettability, and it has been shown that this boundary played a key role in the wetting behavior.[5]

On the other hand, from a microscopic point of view, pioneering studies by Kirkwood and Buff[12] provided the theoretical framework of surface tension based on the statistical mechanics, and molecular dynamics (MD) analysis has been applied for the microscopic understanding of wetting.[13–33] Early study by Nijmeijer et al.[13,14] using mono-atomic Lennard-Jones (LJ) fluid film on a solid surface indicated that the balance in Eq. (1) was applicable. In their work, the liquid-vapor and solid-liquid surfaces were simulated and corresponding interfacial tensions were obtained from the integration of the difference between the pressure tensor components in the surface-normal and surface-lateral directions for the corresponding interfaces. This type of extraction of the interfacial tensions based on Bakker's equation[3,34] is called the mechanical route[35] and has been adopted for several following studies, and most of them indicated that Young's macroscopic model was also applicable to simple mono-atomic liquids at the microscale when the apparent contact angle of an equilibrium droplet on a planer solid surface was used.[15–20] In addition to the mechanical route, a number of new techniques are proposed for the calculation of the solid-related interfacial tensions, including the test-area perturbation method,[21,22] free-energy-based methods using transition matrix Monte Carlo simulations,[23,24] and the thermodynamic integration (TI) by the phantom-wall[25–27] and dry-surface (DS).[28–30] Calculation of interfacial tensions of realistic molecular liquids, e.g., water or hexane, on a complex solid surface was made more approachable by using these methods because the extraction of local distributions of the stress tensor was no longer needed. Interestingly, Young's macroscopic model using the above calculated interfacial tensions sometimes did not give a reasonable estimate of the apparent droplet contact angle for these complex systems, although the reason of this discrepancy was not clear.[31–33] Related to this feature, a very long relaxation time to obtain an equilibrium droplet contact angle was also reported.[33] Two of the present authors have also carried out MD simulations of an argon droplet[20] and a water-alcohol mixture droplet[27,36] on a flat crystal, where we obtained the spatial distribution of the stress tensor in the fluids and extracted the solid-liquid, solid-vapor, and liquid-vapor interfacial tensions γ_{SL}, γ_{SV}, and γ_{LV}, respectively. Although these studies followed the mechanical route, we also obtained the spatial distributions of the stress field instead of merely using the resulting integrals. General questions arose from these studies: whether the mechanical route and other energy-based routes give the same solid-related interfacial tensions γ_{SL} and γ_{LV}, and what kind of condition must be provided for Young's equation to hold.

To make clear these questions, in this study, we carried out at first MD simulations of a hemi-cylindrical Lennard-Jones droplet on a flat and smooth solid surface with focusing on the following three points regarding the mechanical route:

- The original Bakker's equation is intended to be applied only for the liquid-vapor or liquid-gas interface, and whether this equation is really applicable to the solid-related interfacial tensions γ_{SL} and γ_{SV}.
- Regarding the integration interval, where the lower and upper limits of the integration should be.
- We have a variation of choices of the stress tensor: including the liquid-solid component or excluding it, for surface-normal and surface-tangential components in the calculation of the stress tensor close to the solid surface, and which choice gives the proper description of the interfacial tensions.

For these purposes, we examined in detail the surface-lateral force balance exerted on a control volume set around the contact line using the distributions of the fluid stress-tensor components. Then, we related the three interfacial tensions γ_{LV}, γ_{SL}, and γ_{SV} with the fluid stress integral exerted on each face of this control volume with an aid of extended thought experiment for the solid-related interfacial tensions. At this stage, we made the above-mentioned three points clear. Then, we showed that Young's equation was applicable to the present system because the lateral force exerted from the solid surface on the fluid molecules was negligibly small. A proper definition of the droplet contact angle was also provided. Finally, we compared the solid-liquid and solid-vapor interfacial tensions obtained by the mechanical route with the solid-liquid and solid-vapor works of adhesion obtained by the dry-surface method as one of the thermodynamic routes.

II. SIMULATION METHOD

We employed three types of equilibrium simulation systems with respect to flat solid surfaces, as shown in Fig. 1:

(a) droplet system

(b) dry-surface solid-liquid (DS-SL) systems

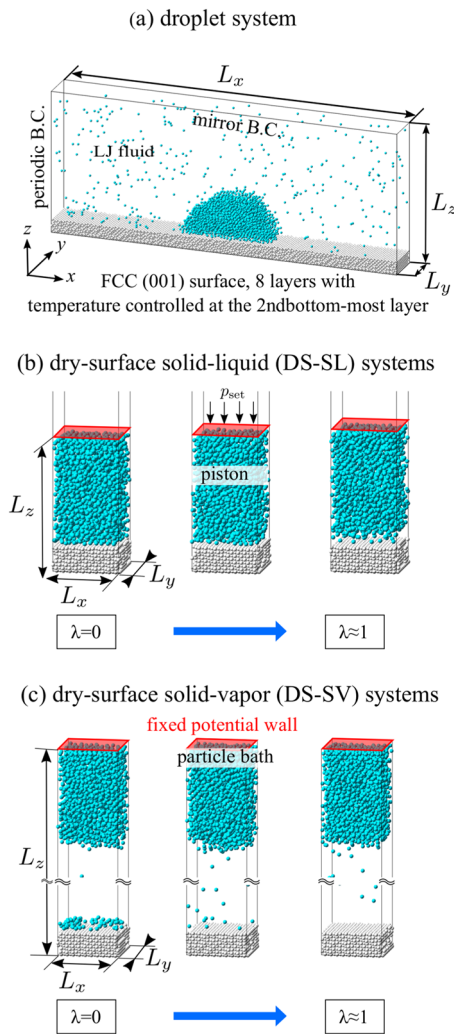(c) dry-surface solid-vapor (DS-SV) systems

FIG. 1. (a) Droplet simulation system with a hemi-cylindrical Lennard-Jones (LJ) droplet on a flat solid surface with an FCC crystal structure. Simulation systems used for the calculation of works of adhesion of the (b) solid-liquid (SL) and (c) solid-vapor (SV) interfaces.

(a) for a hemi-cylindrical droplet on the solid surface, and for the calculation of works of adhesion of the (b) solid-liquid (SL) and (c) solid-vapor (SV) interfaces through the Dry-Surface (DS) method based on the thermodynamic integration (TI). Hereafter, they are denoted by (a) droplet, (b) SL-DS, and (c) SV-DS systems.

A. Potential model

Generic particles interacting through a 12-6 Lennard-Jones potential were adopted as the fluid molecules for ease of physical understanding as in our previous study.[20] The 12-6 LJ potential given by

$$\Phi^{\mathrm{LJ}}(r_{ij}) = \Theta(r_c - r_{ij}) \cdot 4\epsilon \left[\left(\frac{\sigma}{r_{ij}} \right)^{12} - \left(\frac{\sigma}{r_{ij}} \right)^{6} + c_2 \left(\frac{r_{ij}}{r_c} \right)^{2} - c_0 \right] \quad (2)$$

was used for the interaction between fluid molecules, where r_{ij} was the distance between the molecules i at position $\boldsymbol{r}_i$ and j at $\boldsymbol{r}_j$, while ϵ and σ denoted the LJ energy and length parameters, respectively. This LJ interaction was truncated at a cut-off distance of $r_c = 3.5\sigma$, and quadratic functions were added so that the potential and interaction force smoothly vanished at r_c with the Heaviside step function Θ. The constant values of c_2 and c_0 are shown in our previous study.[20] Hereafter, fluid and wall molecules are denoted by "f" and "w," respectively, and the corresponding combinations are indicated by subscripts.

A face-centered cubic (FCC) crystal with an exposed (001) face was used as the solid wall in contact with the fluid, and the interaction potential between wall atoms was expressed by the harmonic potential for the nearest neighbors with an equilibrium distance r_0. The solid-fluid interaction was also expressed by the LJ potential equivalent to Eq. (2), where the length parameter σ_{fw} was given by the Lorentz mixing rule, and the energy parameter ϵ_{fw} was changed in a parametric manner by multiplying a fluid–wall interaction coefficient η to the base value as $\eta\epsilon_{\mathrm{fw}}^0$, where the base value ϵ_{fw}^0 was given by the Berthelot mixing rule as $\epsilon_{\mathrm{fw}}^0 = \sqrt{\epsilon_{\mathrm{ff}}\epsilon_{\mathrm{ww}}}$. The energy parameter ϵ_{fw} was further multiplied by a coupling parameter in the SL-DS and SV-DS systems as described later.

In addition to these intermolecular potentials, we employed a one-dimensional field Φ^{p} for the piston in the SL-DS systems given by

$$\Phi^{\mathrm{p}}(z'_i) = \Theta(\sigma_{\mathrm{fw}} - z'_i) \cdot 4\pi\rho_n\epsilon_{\mathrm{fw}}^0\sigma_{\mathrm{fw}}^2 \left[\frac{1}{5}\left(\frac{\sigma_{\mathrm{fw}}}{z'_i} \right)^{10} - \frac{1}{2}\left(\frac{\sigma_{\mathrm{fw}}}{z'_i} \right)^{4} + \frac{3}{10} \right],$$
$$(3)$$

as a function of the distance $z'_i \equiv z_{\mathrm{p}} - z_i$ between a z-normal plane at $z = z_{\mathrm{p}}$ and fluid molecule i at a height $z = z_i$. This potential field mimicked a mean potential field created by a single layer of solid atoms with a uniform area number density $\rho_n = r_0^{-2}$, and by setting the cut-off distance at σ_{fw}, only repulsive force was exerted on the fluids by this field. We also used a similar one-dimensional field Φ^{b} given by

$$\Phi^{\mathrm{b}}(z''_i) = 4\pi\rho_n\epsilon_{\mathrm{fw}}^0\sigma_{\mathrm{fw}}^2 \left[\frac{1}{5}\left(\frac{\sigma_{\mathrm{fw}}}{z''_i} \right)^{10} - \frac{1}{2}\left(\frac{\sigma_{\mathrm{fw}}}{z''_i} \right)^{4} \right], \quad (4)$$

as a function of the distance $z''_i \equiv z_{\mathrm{b}} - z_i$ between a z-normal plane fixed at $z = z_{\mathrm{b}}$ on the top of the simulation cell and fluid molecule i at a height $z = z_i$. This potential field was used as the particle bath in the SV-DS systems. Further details of the piston and particle bath are described in Sec. II B.

B. Simulation systems

For the droplet system, periodic boundary conditions were set in the x- and y-directions, and a hemi-cylindrically shaped droplet was formed on the solid surface with the droplet axis parallel to the y-axis as shown in Fig. 1(a) so that the effect of line tension[7,8,17,26,37] was neglected. A mirror boundary condition was employed at the top boundary in the z-direction, whereas a solid wall consisting of the FCC

crystal was located on the bottom of the calculation cell which directed its (001) plane normal to the z-direction. This solid wall had eight layers so that possible minimum distance between the argon molecule and wall atom in the bottom layer was longer than the cut-off distance of the fluid-wall interaction potential.

The position of the wall atoms in the bottom layer of the base crystal was fixed, and the temperature of those in the second layer from the bottom, which were sufficiently far from the solid-liquid interface, was controlled by using the standard Langevin thermostat in all directions at a control temperature T_c of 85 K with a Debye temperature of 240 K.[20,38] On the other hand, no direct thermostatting was imposed on the fluid molecules, and the fluid temperature was maintained only through the heat conduction with the solid so that the effects of thermostatting attached to the second-bottom layer of the solid would be negligible on the present equilibrium wetting behavior.

A cylindrical liquid droplet was first equilibrated away from the solid surface, and after its automatic adsorption onto a solid surface followed by a further equilibration run of 20 ns, an initial equilibrium hemi-cylindrical droplet was obtained. The average of 40 ns thereafter was used for the analysis, where we obtained two-dimensional distributions of density and stress components in the frame of reference relative to the center of mass of the droplet, considering that the droplet showed a random Brownian motion without noticeable pinning on the homogeneous and smooth solid surface in this study.

For the SL-DS systems shown in Fig. 1(b), a solid-liquid interface was formed between the liquid and bottom solid wall with the same crystal structure, exposed face, and corresponding wettability parameter η as the droplet system. A periodic boundary condition was employed in lateral x- and y-directions, and the placement and temperature control of the solid surface were the same as in the droplet system, whereas the system width L_x was set smaller since we only dealt with solid-liquid two-phase interface. In addition, we set a piston above the liquid to attain a constant pressure. This piston interacted with the fluid molecules with the potential Φ^p given in Eq. (3), and its height z_p obeyed the following equation of motion:

$$m_p \frac{d^2 z_p}{dt^2} = A(p - p_{set}), \qquad (5)$$

where m_p, A, p, and p_{set} denoted the mass of the piston, surface area ($=L_x L_y$), system, and control pressures, respectively. The system pressure p was obtained from the total normal force exerted on the piston from argon molecules given by

$$p = -\frac{1}{A} \frac{\partial}{\partial z_p} \sum_i^{N_f} \Phi^p(z'_i), \qquad (6)$$

where N_f was the number of fluid molecules. By allocating a sufficient number of fluid molecules and by setting the pressure p_{set} above the vapor pressure, a liquid bulk with a constant density was formed between the solid wall and piston. We also applied the Nosé-Hoover thermostat[39] only to the

fluid molecules to maintain the system temperature at T_c, which was the same as the control temperature for the solid, to maintain a constant fluid temperature even in case the fluid and solid were almost non-interacting during the DS procedure described in Sec. II D. The relaxation time of the thermostat was 1 ps. Note that the effects of this thermostat on the DS procedure were negligibly small because the present SL-DS system was in equilibrium.

The interaction energy parameter ϵ_{fw} was multiplied by the coupling parameter $1 - \lambda$ in this system for the dry-surface scheme, and we obtained multiple equilibrium systems with various λ values with $0 \leq \lambda < 1$ to numerically calculate the thermodynamic integration, as described in Sec. II D. Each system was obtained after a preliminary equilibration over 5 ns, and the time average of 20 ns was used for the analysis.

For the SV-DS systems, we investigated the interfacial energy between saturated vapor and corresponding solid surface set on the bottom of the simulation cell by placing an additional particle bath on the top, as shown in Fig. 1(c). The setup regarding the periodic boundary conditions employed in lateral x- and y-directions, temperature control and placement conditions for the solid surface, and additional Nosé-Hoover thermostat for the fluid molecules were the same as the SL-DS system, whereas the particle bath was kept in place by the potential field Φ^b in Eq. (4) at a fixed height sufficiently far from the solid surface. Note that the potential field mimicked a completely wettable surface with an equilibrium contact angle of zero with the present potential parameters, i.e., a liquid film was formed on the particle bath. With this setting, a solid-vapor interface with the same density distribution as that in a droplet system was achieved. We formed multiple equilibrium systems with various values of the coupling parameter λ with the same recipe as the SL-DS systems.

The velocity Verlet method was applied for the integration of the Newtonian equation of motion with a time increment δt of 5 fs for all systems. Values of the simulation parameters are summarized in Table I with the corresponding non-dimensional ones, which are normalized by the corresponding standard values. Note that the η value ranged up to 0.5 for the droplet systems because the system with η = 0.6 showed complete wetting and no hemi-cylindrical droplet was formed.

C. Calculation of fluid stress distribution

For the droplet system, we extracted the distribution of the two-dimensional fluid stress tensor averaged in the axial direction. The method of plane (MoP) was adopted in the present study instead of using the volume average (VA) used in the previous study[20,27] because the exact balance satisfied for an arbitrary control volume bounded by a closed surface was one of the most important prerequisites of the formulation in this study. Note that we extracted the fluid stress as an internal force while considering all solid contributions to be an external force field[14,40,41] in this study. The local fluid stress tensor $\tau(x, z)$ was calculated by dividing the system into x- and z-normal flat bin faces with a width of 0.08 nm for both.

TABLE I. Simulation parameters and their corresponding non-dimensional values.

Property	Value	Unit	Non-dim. value
σ_{ff}	0.340	nm	1
σ_{ww}[a]	0.350	nm	1.03
σ_{fw}	$(\sigma_{\text{ff}} + \sigma_{\text{ww}})/2$		
ϵ_{ff}	1.67×10^{-21}	J	1
ϵ_{ww}[b]	1.000×10^{-21}	J	0.599
ϵ_{fw}^0	$\sqrt{\epsilon_{\text{ff}}\epsilon_{\text{ww}}}$		
ϵ_{fw}	$\eta\epsilon_{\text{fw}}^0$		
η	0.1–0.6 (0.5 for droplet)	...	...
m_f	6.63×10^{-26}	kg	1
m_w	32.4×10^{-26}	kg	4.88
m_p	4.54×10^{-22}	kg	6.84×10^3
r_0 (FCC)	0.277	nm	0.815
k	46.8	N/m	3.24×10^3
T_c	85	K	0.703
N_f (droplet)	3000	...	...
N_f (DS-SL)	2000	...	...
N_f (DS-SV)	2000	...	...
L_x (droplet)	39.2	nm	1.15×10^2
L_x (DS-SL, DS-SV)	3.92	nm	11.5
L_y	3.92	nm	11.5
L_z (droplet)	16.0	nm	47.1
L_z (DS-SL)	9.80–9.85	nm	28.8–29.0
L_z (DS-SV)	20.0	nm	58.8
p_{set} (DS-SL)	1.00×10^6	nm	2.35×10^{-2}

[a]Used only for the Lorentz mixing rule.
[b]Used only for the Berthelot mixing rule.

The fluid stress tensor component $\tau_{\alpha\beta}$, which expresses the stress in the β-direction exerted on a surface element with an outward normal in the α-direction, is given by kinetic term $\tau_{\alpha\beta}^{\text{kin}}$ and inter-molecular interaction term $\tau_{\alpha\beta}^{\text{int}}$ as

$$\tau_{\alpha\beta} = \tau_{\alpha\beta}^{\text{kin}} + \tau_{\alpha\beta}^{\text{int}}. \tag{7}$$

In the MoP, the kinetic term on an α-normal bin face with an area A_α was calculated by

$$\tau_{\alpha\beta}^{\text{kin}} = -\frac{1}{A_\alpha}\left\langle \sum_{i\in\text{fluid},\delta t}^{\text{across}A_\alpha} \frac{(2\Theta(\boldsymbol{v}_i \cdot \boldsymbol{e}_\alpha)-1)m_i\boldsymbol{v}_i \cdot \boldsymbol{e}_\beta}{\delta t} \right\rangle, \tag{8}$$

where m_i and $\boldsymbol{v}_i$ denoted the mass and velocity vector of the ith fluid molecule, and $\boldsymbol{e}_\alpha$ and $\boldsymbol{e}_\beta$ were the unit normal vectors in α- and β-directions, respectively. The angular brackets denoted the time average, and the summation $\sum_{i,\delta t}^{\text{across}A_\alpha}$ was taken for every fluid molecule i passing through the bin face within a time interval of δt, which was equal to the time increment for the numerical integration. A switching function, $2\Theta(\boldsymbol{v}_i \cdot \boldsymbol{e}_\alpha) - 1$, where Θ was the Heaviside step function, giving ± 1 depending on the sign of $\boldsymbol{v}_i \cdot \boldsymbol{e}_\alpha$ was included through the Heaviside step function Θ in the RHS of Eq. (8). Strictly speaking, the velocity $\boldsymbol{v}_i$ in Eq. (8) should be a relative one to the average; however, we did not use the relative velocity considering that the average velocity of the droplet under random Brownian motion was sufficiently small.

On the other hand, the intermolecular interaction term in Eq. (7) was given by

$$\tau_{\alpha\beta}^{\text{int}} = -\frac{1}{A_\alpha}\left\langle \sum_{(i,j)\in\text{fluid}}^{\text{across}A_\alpha} \left(2\Theta(\boldsymbol{r}_{ij} \cdot \boldsymbol{e}_\alpha)-1\right)\boldsymbol{f}_{ij} \cdot \boldsymbol{e}_\beta \right\rangle, \tag{9}$$

where $\boldsymbol{r}_{ij}$ and $\boldsymbol{f}_{ij}$ denoted the relative position vector $\boldsymbol{r}_j - \boldsymbol{r}_i$ and force vector exerted on molecule j at position $\boldsymbol{r}_j$ from molecule i at $\boldsymbol{r}_i$, respectively, and the summation $\sum_{(i,j)\in\text{fluid}}^{\text{across}A_\alpha}$ was taken for all line segments between $\boldsymbol{r}_i$ and $\boldsymbol{r}_j$ which crossed the bin face. Note that technically the fluid-solid interaction can also be included as $i - j$ pair in the summation $\sum_{(i,j)}^{\text{across}A_\alpha}$ in Eq. (9), but only the fluid-fluid interaction was taken into account as the fluid stress as the internal force, and fluid-solid contribution was considered as an external force field in this study, as mentioned above.[14,40,41] This will be discussed in detail in Sec. III A. Note that Eqs. (8) and (9) have a negative sign because they express stress, whose diagonal component is pressure with inverted sign. For example, Eq. (8) always has a non-positive diagonal stress value, i.e., positive pressure value, because molecules passing always transfer moment, which results in pressure force directed towards the control surface from either side. On the other hand, Eq. (9) can be both negative and positive, where a negative diagonal stress, i.e., positive pressure, indicates that two molecules on opposing sides are repulsing each other, while the opposing sign indicates that the molecules are attracting each other.

D. Works of adhesion of solid-liquid and solid-vapor interfaces

Leroy and Müller-Plathe[28] proposed the Dry-Surface method in which the coupling parameter for the thermodynamic integration (TI)[42] was embedded in the fluid-wall interaction parameter. They formed a solid-liquid interface at first, and then by turning off the attractive part of the fluid-wall interaction potential through the coupling parameter, the work of adhesion was extracted through the thermodynamic integration along a reversible path. In the present study, we adopted the DS method for the SL interface and for the SV interface as shown in Figs. 1(b) and 1(c), respectively. A coupling parameter λ was embedded in the fluid-wall interaction potential for both systems as

$$\Phi_{\text{fw}}^{\text{DS}}(r_{ij}, \lambda) = (1 - \lambda)\Phi_{\text{fw}}^{\text{LJ}}(r_{ij}), \tag{10}$$

where $\Phi_{\text{fw}}^{\text{LJ}}(r_{ij})$ denoted the LJ interaction in Eq. (2).

For the case of SL-DS in Fig. 1(b), we obtained equilibrium solid-liquid interfaces with discrete coupling parameter λ from 0 to 0.999. With the setup described in Subsection II B, the number of molecules N, pressure p, and temperature T were kept constant, i.e., we formed constant NpT systems. Note that the maximum value of λ was set slightly below 1 to keep the solid-fluid interaction to be effectively only repulsive. This value is denoted by 1^- hereafter. The SL interface at $\lambda = 0$ with $\Phi_{\text{fw}}^{\text{DS}}(r_{ij}, \lambda) = \Phi_{\text{fw}}^{\text{LJ}}(r_{ij})$ was separated into solid-vacuum and liquid-vacuum interfaces by changing the coupling parameter to $\lambda = 1^-$ as shown in left and right panels

of Fig. 1(b), as no fluid molecules were adsorbed onto the solid surface because the fluid-wall interaction was almost without attraction at $\lambda = 1^-$. Hence, the difference of the Gibbs free energy $\Delta G \equiv G|_{\lambda=1^-} - G|_{\lambda=0}$ between systems at $\lambda = 0$ and $\lambda = 1^-$ under constant NpT was related to the difference in the surface interfacial energies as

$$W_{SL} \equiv \frac{\Delta G}{A} = \gamma_{S0} + \gamma_{L0} - \gamma_{SL}$$
$$\approx \gamma_{S0} + \gamma_{LV} - \gamma_{SL}, \qquad (11)$$

where the vacuum phase was denoted by subscript "0" and γ_{S0} and γ_{L0} were the solid-vacuum and liquid-vacuum interfacial energies per unit area. Note that γ_{L0} was substituted by the liquid-vapor interfacial tension γ_{LV} in the final approximation considering that the vapor density was negligibly small. The work of adhesion W_{SL} was defined by the minimum work needed to strip the liquid from the solid surface per area under constant NpT.

Using the NpT canonical ensemble associated with the Gibbs free energy G, the difference of the Gibbs free energy ΔG in Eq. (11) was calculated through the following TI:

$$\Delta G = \int_0^{1^-} \frac{dG(\lambda)}{d\lambda} d\lambda = \int_0^{1^-} \left\langle \frac{\partial H}{\partial \lambda} \right\rangle d\lambda + \int_0^{1^-} p_{set} \left\langle \frac{\partial V}{\partial \lambda} \right\rangle d\lambda$$
$$= -\int_0^{1^-} \left\langle \sum_{i \in \text{fluid}}^{N_f} \sum_{j \in \text{wall}}^{N_w} \Phi_{fw} \right\rangle d\lambda + A p_{set} \left(\langle z_p|_{\lambda=1^-} \rangle - \langle z_p|_{\lambda=0} \rangle \right), \quad (12)$$

where H and V are the Hamiltonian, i.e., internal energy of the system and system volume, respectively, and N_w is the number of wall molecules. The ensemble average was substituted by the time average in the simulation and was denoted by the angular brackets.

On the other hand, for the case of SV-DS in Fig. 1(c), we simulated constant-temperature equilibrium systems of a fixed volume with a particle bath located on the top for coupling parameter λ ranging from 0 to 1^-. The SV interface in the SV-DS system at $\lambda = 0$ in the left panel of Fig. 1(c) was in equilibrium with a saturated vapor at this temperature and this approximately represented the SV interface away from the contact line in the droplet system with the corresponding η value. Similar to the SL-DS systems, the SV interface at $\lambda = 0$ was divided into S0 and V0 interfaces at $\lambda = 1^-$ as shown in Fig. 1(c), while the SV-DS systems were under constant NVT. Thus, the solid-vapor work of adhesion W_{SV} was given by the difference of the Helmholtz free energy ΔF per unit area and was related to the difference in the surface interfacial energy as

$$W_{SV} \equiv \frac{\Delta F}{A} = \gamma_{S0} + \gamma_{V0} - \gamma_{SV}$$
$$\approx \gamma_{S0} - \gamma_{SV}, \qquad (13)$$

where γ_{V0} was set zero in the final approximation.

Using the NVT canonical ensemble, ΔF in Eq. (13) was calculated through the TI as

$$\Delta F = \int_0^{1^-} \frac{\partial F(\lambda)}{\partial \lambda} d\lambda = \int_0^{1^-} \left\langle \frac{\partial H}{\partial \lambda} \right\rangle d\lambda$$
$$= -\int_0^{1^-} \left\langle \sum_i^{N_f} \sum_j^{N_w} \Phi_{fw}^{LJ}(r_{ij}) \right\rangle d\lambda. \qquad (14)$$

III. RESULTS AND DISCUSSION

A. Force balance on a control volume around a contact line

Figure 2 displays the time-averaged density distribution of an equilibrium argon droplet in the case of $\eta = 0.4$, where the origin of the x-axis was set relative to the droplet center of mass. As well-known, multiple adsorption layers with a thickness about 1-2 nm were formed at the solid-liquid interface, and a hemi-cylindrical liquid-vapor interface with a uniform curvature was observed above. This indicated that the liquid-vapor interfacial tension was uniform except around the contact line. We supposed a rectangular control volume set around the contact line with its bottom and top faces parallel to the solid surface and its vertical left face in the center of mass of the droplet as shown in Fig. 2 and examined the horizontal force balance on this control volume through the fluid stress tensor field $\tau(x, z)$. Before examining the details of the control volume, we will look at the fluid stress on $x = 0$.

Figure 3 shows the distributions of the fluid stress components $\tau_{xx}(0, z)$ and $\tau_{zz}(0, z)$ in the center of the droplet, i.e., $\tau(x, z)|_{x=0}$, superimposed with the distribution of density $\rho(0, z)$. With respect to the relation between ρ and τ_{xx}, the former fluctuated near the solid due to the multi-layered structure, and τ_{xx} also fluctuated corresponding to the density: negative in the high density layers and positive in between. These were because the fluid was compressed in the lateral directions inside the adsorption layers and attractive force lines acting between fluid molecules in neighbouring adsorption layers crossed the x-normal bin faces in between. Above these adsorption layers, ρ and τ were both constant, indicating
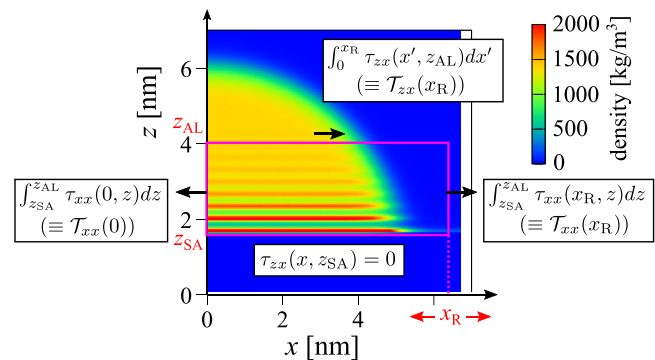

FIG. 2. Time-averaged density distribution of an equilibrium argon droplet with a fluid-wall interaction parameter η of 0.4 used as an example system for the analysis of horizontal force balance exerted on a rectangular control volume, shown in magenta, set around the contact line.
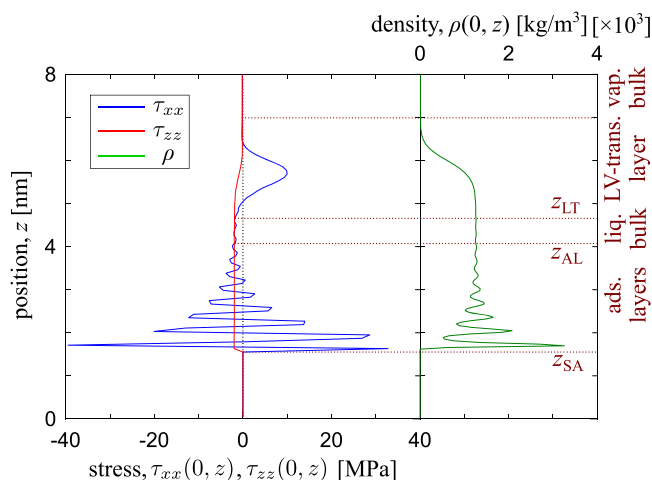
FIG. 3. Distributions of the (left) fluid stress components $\tau_{xx}(x, z)$ and $\tau_{zz}(x, z)$, and (right) density $\rho(x, z)$ on the central plane of the droplet at $x = 0$. The vertical axis is shared for the left and right graphs, and each region is categorized on the right side based on these distributions.

that a liquid bulk was formed. Note that the negative value of τ_{xx} was due to the Laplace pressure. In contrast to the gradual decrease of density from liquid to vapor, τ_{xx} showed a remarkable peak structure in the transition layer between liquid and vapor, which corresponded to the surface tension. A saturated vapor bulk with constant density and τ_{xx} existed above the liquid-vapor interface.

On the other hand, τ_{zz} was only equal to τ_{xx} in the liquid and vapor bulks, i.e., the fluid stress was isotropic. In contrast to τ_{xx} which fluctuated in the adsorption layers, τ_{zz} was almost constant. This was because the strong external force from the solid was exerted only near the solid surface, and the force balance normal to the solid surface was satisfied only with τ_{zz} since the contribution from τ_{xz} cancelled out due to the symmetric feature of this area. Indeed, based on linear momentum conservation in a steady state system without any flow perpendicular to the wall, $\partial \tau_{zz}/\partial z = 0$ is satisfied in case without external force. An equivalent explanation for this is that the oscillations in the kinetic and interaction stress profiles cancel out each other for τ_{zz}. This was not the case near the solid surface where the external force from the solid was included in the force balance.[41] In other words, the pressure exerted on the fluids there from the liquid bulk, i.e., negative of surface-normal fluid stress, balanced the external force from the solid. Throughout the liquid-vapor transition layer, τ_{zz} showed a simple change between constant bulk values, which was also in contrast to τ_{xx}.

Considering this feature of density and fluid stress distributions, we defined the position of the bottom and top faces of the control volume in the z-direction in Fig. 2 as follows: the former denoted by z_{SA} was set at the boundary of solid and first adsorption layer. More specifically, it was at the position where the liquid density showed steep rise from zero as shown in Fig. 3, corresponding to the nearest limit to the solid

wall the fluid molecules could reach. On the other hand, we set the top face position z_{AL} above the top adsorption layer and below the liquid bulk, as displayed in Fig. 3. Different from z_{SA}, z_{AL} cannot be strictly determined. Actually, we only need strict definition of z_{SA}, whereas z_{AL} may shift into the liquid bulk. This will be mentioned in Sec. III C with the mechanical definition of the contact angle related to the extended Bakker's equation. In addition, we set z_{LT} between the liquid bulk and LV-transition layer. The position of the right face of the control volume was set as a parameter and was denoted by x_R.

Now, we suppose an arbitrary volume V containing only fluid molecules bounded by a closed surface S in the present quasi-two-dimensional droplet system. Exact force balance must be satisfied for the present quasi-static system, and it follows for the surface integral of the fluid stress and volume integral of the external force that

$$\int_S \tau_{ji}(x,z)n_j dS + \iint_V f_i^{ext}(x,z)dV = 0, \quad (15)$$

where the Einstein notation is used with a dummy index j, and $\tau_{ji}(x, z)$, n_j, and $f_i^{ext}(x, z)$ are the fluid stress tensor, unit normal vector of the surface element dS, and external force vector per volume from the solid, respectively. By applying Eq. (15) to the rectangular control volume shown in Fig. 2 with bottom, top, and left positions fixed at $z = z_{SA}$, $z = z_{AL}$, and $x = 0$, respectively, the horizontal component of the LHS of Eq. (15) was given as a function of only x_R, and the first term is written as

$$\int_{S(x_R)} \tau_{jx}(x,z)n_j dS = \int_{z_{SA}}^{z_{AL}} \tau_{xx}(x_R,z)dz - \int_{z_{SA}}^{z_{AL}} \tau_{xx}(0,z)dz + \int_0^{x_R} \tau_{zx}(x,z_{AL})dx, \quad (16)$$

where the three terms in the RHS denoted the fluid stress surface integrals on the right, left, and top faces, respectively. Note that the integral $\int_0^{x_R} \tau_{zx}(x, z_{SA})dx$ was omitted because $\tau_{zx}(x, z_{SA})$ was zero in the entire region of the bottom face because no fluid molecules existed under this plane to contribute to the sum in Eqs. (8) and (9). For short notation, we define the horizontal components of the fluid stress surface integrals in Eq. (16) by

$$\mathcal{T}_{xx}(x) \equiv \int_{z_{SA}}^{z_{AL}} \tau_{xx}(x,z)dz \quad (17)$$

and

$$\mathcal{T}_{zx}(x) \equiv \int_0^x \tau_{zx}(x',z_{AL})dx', \quad (18)$$

as a function of x, and rewrite Eq. (16) as

$$\int_{S(x_R)} \tau_{jx}(x,z)n_j dS = \mathcal{T}_{xx}(x_R) - \mathcal{T}_{xx}(0) + \mathcal{T}_{zx}(x_R). \quad (19)$$

Figure 4 shows the horizontal component of the fluid stress surface integrals for right face $\mathcal{T}_{xx}(x_R)$ and top faces $\mathcal{T}_{zx}(x_R)$ and total surface integral $\mathcal{T}_{xx}(x_R) - \mathcal{T}_{xx}(0) + \mathcal{T}_{zx}(x_R)$ in Eq. (19) for the control volume in Fig. 2 as a function of the right face position x_R, where x_R ranged from the center of
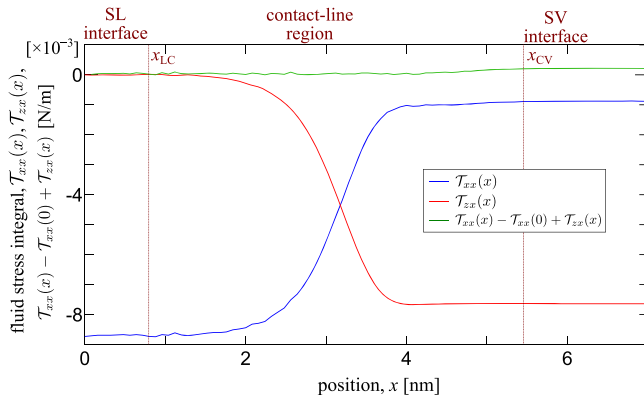
FIG. 4. Horizontal components of the integrated fluid stress $\mathcal{T}_{xx}(x_R) \equiv \int_{z_{SA}}^{z_{AL}} \tau_{xx}(x_R, z)dz$ and $\mathcal{T}_{zx}(x_R) \equiv \int_0^{x_R} \tau_{zx}(x, z_{AL})dx$ acting on the right and top faces of the control volume in Fig. 2 [see Eq. (16)], respectively, as a function of the position of the right face x_R. The total surface integral in Eq. (16) is shown as well, and each region is denoted on the top based on these fluid stress integrals.

the droplet to the solid-vapor interface away from the contact line. It was indicated that

$$\mathcal{T}_{xx}(x_R) - \mathcal{T}_{xx}(0) + \mathcal{T}_{zx}(x_R) \approx 0 \qquad (20)$$

was satisfied in the entire range of x_R even though $\mathcal{T}_{xx}(x_R)$ and $\mathcal{T}_{zx}(x_R)$ changed depending on x_R. By inserting this result into Eq. (15), it followed for the second term of the LHS that

$$\iint_{V(x_R)} f_x^{ext}(x, z)dV \approx 0, \qquad (21)$$

meaning that the horizontal component of the external force was zero irrespective of x_R, i.e., no horizontal force was exerted on the fluid from the solid surface with a densely packed crystal structure everywhere as a time-average for the present droplet system under random Brownian motion even though the fluid density was not uniform. Note that the LHS of Eq. (20) was not exactly zero, and this seemed to be due to the slight roughness of the present solid surface. In the following discussion, we set

$$\mathcal{T}_{xx}(x_R) - \mathcal{T}_{xx}(0) + \mathcal{T}_{zx}(x_R) = 0 \qquad (22)$$

and

$$\iint_{V(x_R)} f_x^{ext}(x, z)dV = 0, \qquad (23)$$

for simplicity.

With respect to $\mathcal{T}_{zx}(x_R)$, its value was zero up to around $x_R = 1$ nm, and this indicated that $\tau_{zx}(x, z_{AL})$ was equal to zero because the fluid stress in the liquid was isotropic up to the liquid-vapor transition layer. After the decrease of $\mathcal{T}_{zx}(x_R)$ with the increase of x_R, it took a constant value above about $x_R = 4$ nm because the fluid stress was isotropic with $\tau_{zx}(x, z_{AL}) = 0$ in the vapor bulk far from the transition layer. Along with the change of $\mathcal{T}_{zx}(x_R)$, the fluid stress integral $\mathcal{T}_{xx}(x_R)$ was constant except in the liquid-vapor transition layer while satisfying Eq. (22) in the entire region as mentioned above.

Considering this feature, we defined the contact line region as $x_{LC} \leq x_R \leq x_{CV}$ between solid-liquid and solid-vapor interfaces in which $\mathcal{T}_{zx}(x_R)$ and $\mathcal{T}_{xx}(x_R)$ changed, as shown in Fig. 4. The definitions of x_{LC} and x_{CV} are not strict; however, the only necessary conditions for the positions (x_{LC}, z_{AL}) and (x_{CV}, z_{AL}) are that the two points are in the liquid and vapor bulks, respectively, to apply the extended Bakker's equation mentioned in Sec. III B. In the following, $\mathcal{T}_{xx}(x_{LC})$ and $\mathcal{T}_{xx}(x_{CV})$ are related with the solid-liquid and solid-vapor interfacial tensions through extending the thought experiment leading to Bakker's equation.

B. Bakker's equation extended to solid-related interfaces

As displayed in Fig. 3, the fluid stress tensor is not isotropic at phase interfaces. Bakker's equation describes the relation between the fluid stress anisotropy and surface tension through a thought experiment shown in Fig. 5(a).[34] In this thought experiment, one piston is set normal to a flat
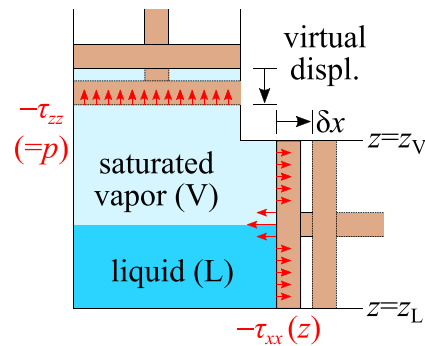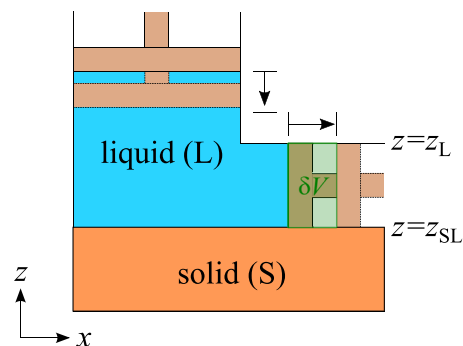

FIG. 5. (a) Thought experiment of Bakker's equation for a flat liquid-vapor interface and (b) that extended for a flat solid-liquid interface. The red arrows denote the pressure, i.e., normal fluid stress with its sign inverted, acting on the piston.

liquid-vapor interface and it covers from $z = z_L$ to $z = z_V$ at liquid and vapor bulk regions, respectively, across the plane of the liquid-vapor interface. Another piston parallel to the interface is set in vapor bulk far from the interface. Through simultaneous virtual infinitesimal displacements of the pistons, only the interface area can be changed without changing the vapor and liquid volumes. Let l be the depth normal to the xz-plane, and $-\delta V$ and δx be the infinitesimal volume change given by the downward displacement of the top piston and corresponding displacement of the side piston, respectively, it follows that

$$\delta V = l\delta x \int_{z_L}^{z_V} dz. \qquad (24)$$

Assuming that this displacement is done quasi-statically under constant temperature, the minimum mechanical work δW required for this change is associated with the change in the Helmholtz energy F given by

$$\delta F \equiv \delta W = -\tau_{zz}\delta V + l\delta x \int_{z_L}^{z_V} \tau_{xx}(z)dz, \qquad (25)$$

where τ_{zz} and τ_{xx} are the surface normal fluid stress components at the surfaces of top and side pistons, respectively. The former is constant in the entire region because of the force balance in the z-direction. We denote this constant value by τ^{bulk}, which is equal to the saturated vapor pressure with its sign inverted. On the other hand, the latter is a function of z, while it is also equal to τ^{bulk} in the liquid and vapor bulks. By equating δF with surface free energy of area $l\delta x$, and eliminating δV, l, and δx with Eq. (24), it follows for the surface tension γ_{LV} that

$$\gamma_{LV} \equiv \left(\frac{\partial F}{\partial A_{LV}}\right)_{N,V,T} = \int_{z_L}^{z_V} \left(\tau_{xx}(z) - \tau^{bulk}\right)dz, \qquad (26)$$

where A_{LV} is the area of the liquid-vapor interface. The integration range in Eq. (26) is sometimes expressed by $\int_{-\infty}^{\infty}$; however, the necessary condition for this range is that z_L and z_V cover the entire range of the interface with anisotropic fluid stress, i.e., between liquid and vapor bulks.

We extend this thought experiment to the solid-liquid interface as shown in Fig. 5(b), where the top piston parallel to the interface is set away from the interface, whereas the side piston is set not across the plane of the interface but just on it so that the piston face can only contact the liquid. Then, one can achieve similar simultaneous infinitesimal displacements of the pistons without changing the liquid volume. However, the resulting change in the interface is not a simple increase of the SL interface area but a replacement of the solid-vacuum interface with the SL interface. Hence, the relations among the minimum mechanical work, change in the free energy and interfacial tensions are expressed by

$$\gamma_{SL} - \gamma_{S0} \equiv \left(\frac{\partial F}{\partial A_{SL}}\right)_{N,V,T} = \int_{z_{SL}}^{z_L} \left(\tau_{xx}(z) - \tau^{bulk}\right)dz. \qquad (27)$$

Note that the lower limit of the integration range should be defined physically at the limit nearest to the solid which the fluid can reach, i.e., exactly the same as z_{SA} microscopically defined in Fig. 3.

If we consider another thought experiment system of the solid-vapor interface similar to Fig. 5(b), the following relation is derived:

$$\gamma_{SV} - \gamma_{S0} \equiv \left(\frac{\partial F}{\partial A_{SV}}\right)_{N,V,T} = \int_{z_{SV}}^{z_V} \left(\tau_{xx}(z) - \tau^{bulk}\right)dz. \qquad (28)$$

The difference from γ_{S0} described in Eqs. (27) and (28) was called "relative" interfacial tensions in our previous studies.[20,27]

C. Relation between Young's equation and extended Bakker's equation

Now we go back again to the horizontal force balance exerted on the control volume around the contact line. From Fig. 4, it was known that $\mathcal{T}_{xx}(x_R)$ and $\mathcal{T}_{zx}(x_R)$ were both constant for $0 \le x_R \le x_{LC}$ and $x_R \ge x_{CV}$ away from the contact line. Thus, from Eqs. (17)–(19) and (22), it follows that

$$\int_{z_{SA}}^{z_{AL}} \tau_{xx}(x_{CV},z)dz - \int_{z_{SA}}^{z_{AL}} \tau_{xx}(x_{LC},z)dz + \int_{x_{LC}}^{x_{CV}} \tau_{zx}(x,z_{AL})dx = 0. \qquad (29)$$

In order to think about the third term of Eq. (29), at first, we suppose an imaginary equilibrium cylindrical liquid pillar having the same radius of curvature R as the LV interface of the droplet on the solid surface as shown in Fig. 6 and consider the horizontal force balance on a rectangular control volume whose bottom face is on the x-axis at $z = 0$ depicted in blue. Then, the shear stress on the bottom face $\tau_{zx}(x,0)$ is zero because of the symmetry there, and it follows that

$$z_{AL}p_{int} - z_{AL}p_{ext} + \int_{x_{LC}}^{x_{CV}} \tau_{zx}(x,z_{AL})dx = 0, \qquad (30)$$

where the 1st and 2nd terms are the horizontal force per unit depth exerted on the left and right faces expressed by constant external and internal pressures p_{ext} and p_{int}, whereas the 3rd term is that on the top faces. Note that p_{int} and p_{ext} are equal to the uniform normal fluid stress $-\tau_{xx}$ in the liquid and
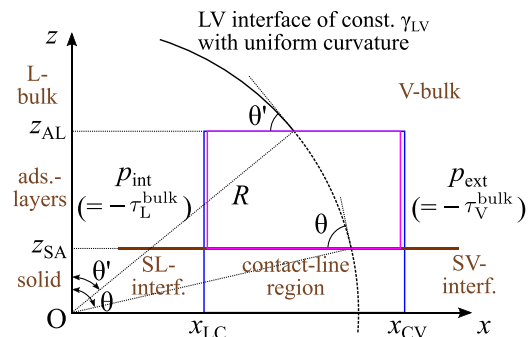

FIG. 6. (Magenta) schematic of the control volume set around the contact line of a quasi-two-dimensional hemi-cylindrical droplet on a flat and smooth solid surface at $z = z_{SA}$, shown in brown. (Blue) additional control volume set for an imaginary cylindrical droplet having the same radius of curvature as the hemi-cylindrical droplet.

vapor bulk regions, respectively. Let θ' be the angle between the top face and LV interface shown in Fig. 6, for which the geometric relation is given by

$$\cos \theta' = \frac{z_{AL}}{R}. \tag{31}$$

By applying Eq. (31) and Young-Laplace equation

$$\Delta p \equiv p_{int} - p_{ext} = \frac{\gamma_{LV}}{R}, \tag{32}$$

it follows for Eq. (30) that

$$\int_{x_{LC}}^{x_{CV}} \tau_{zx}(x, z_{AL}) dx = -\gamma_{LV} \cos \theta', \tag{33}$$

indicating that the integral of the fluid shear stress on the top face is equivalent to the lateral force exerted by the LV surface tension.

Now, we go back to Eq. (29). Let τ_V^{bulk} and τ_L^{bulk} be the isotropic fluid stress values in the vapor and liquid bulks equal to $-p_{ext}$ and $-p_{int}$, respectively, and by once removing them from the integrand of the first and second terms of the LHS of Eq. (29), and by adding their integrals, it follows that

$$\int_{z_{SA}}^{z_{AL}} \left(\tau_{xx}(x_{CV}, z) - \tau_V^{bulk} \right) dz - \int_{z_{SA}}^{z_{AL}} \left(\tau_{xx}(x_{LC}, z) - \tau_L^{bulk} \right) dz$$
$$+ (z_{AL} - z_{SA})(p_{int} - p_{ext}) - \gamma_{LV} \cos \theta' = 0. \tag{34}$$

Note that when Eq. (23) is satisfied, Eq. (29) would hold even if the lower limit of the integral for the 1st and 2nd term of LHS was taken at an arbitrary position below z_{SA} because $\tau_{xx}(x, z) = 0$ for $z < z_{SA}$. Even in this case, Eq. (34) is also recovered, as shown in Appendix A. By substituting the 1st and 2nd term with the left-most hand sides of Eqs. (28) and (27), respectively, Eq. (34) is rewritten as

$$\gamma_{SV} - \gamma_{SL} - \gamma_{LV} \cos \theta' + (z_{AL} - z_{SA}) \Delta p = 0, \tag{35}$$

indicating that the interfacial tensions are balanced on the control volume including the Laplace pressure. Finally, let θ be the angle between the bottom face and extended cylindrical plane of the LV interface satisfying

$$\cos \theta = \frac{z_{SA}}{R}, \tag{36}$$

as shown in Fig. 6, and by using Eq. (31) and Young-Laplace equation (32), Eq. (35) recovers Young's equation (1).

The following three points used to derive this consequence should be rephrased here. One point is that this result is derived because Eq. (23) is satisfied on the present flat and smooth solid surface as a prerequisite. In other words, this equivalence of Young's equation to the pure mechanical balance is true only when Eq. (23) holds, and it is not the case for a contact line subject to pinning due to physical or chemical inhomogeneity, e.g., surface roughness, edge structures, impurities, or surface deformation also seen in our case in Fig. 4. This condition of Eq. (23) would easily be violated for a water droplet on an inhomogeneous polar solid surface because the average dipole direction of water molecules at the

contact line would be biased from the surface normal direction.[22,24,31-33,36] Note that Kanduč and Netz[31] showed a good agreement for contact angles of water on a homogeneous polar surface calculated from their interface potential method and droplet simulation. Extracting the lateral force around the contact line could provide further insight into the matter and will be the target of future research. The second point is that Eq. (29) holds even though the lower limit of the integral for the 1st and 2nd term of LHS is taken below z_{SA} on condition that Eq. (23) is satisfied, whereas z_{SA} must be strictly given by Eqs. (27) and (28), which determines γ_{SL} and γ_{SV}, respectively. Thus, the position of the fluid-wall interface to define the contact angle θ is also determined. This is because different values of isotropic fluid stress values τ_V^{bulk} and τ_L^{bulk}, whose difference corresponds to the Laplace pressure, are included to derive γ_{SL} and γ_{SV} in Eq. (34). This is not the case for a contact line with the flat LV interface for which the fluid-wall interface does not have to be given to define the contact angle. We show in Appendix B that Eq. (33) holds also in this case with $\theta' = \theta$. Note also that the fluid-wall interface position z_{SA} may include ambiguity in case the surface is not flat. The third point is that the top face position set at z_{AL} in Eq. (29) is not an essential prerequisite, and it may be varied between z_{AL} and z_{LT}. In other words, Young's equation should not be considered as the horizontal force balance on a point as in Eq. (1), but on a finite volume as in Eq. (35).[43]

D. Relation between extended Bakker's equations and work of adhesion

We have extended Bakker's equation to SL and SV interfacial tensions and examined Young's equation from a mechanical point of view above. In Fig. 7, we compared these interfacial tensions obtained from a mechanical route with the corresponding work of adhesion W_{SL} and W_{SV} obtained from a thermodynamic route using the TI. Note that the error-bar for W_{SV} became larger for larger η because of the fluctuating behavior of the solid-vapor adsorption layer. Considering the difference of the definitions, relative interfacial tensions $\gamma_{SL} - \gamma_{S0}$ and $\gamma_{SV} - \gamma_{S0}$ are shown as $-(\gamma_{SL} - \gamma_{S0}) + \gamma_{LV}$ and $-(\gamma_{SV} - \gamma_{S0})$, respectively, where $\gamma_{LV} = 11.3 \times 10^{-3}$ N/m is added to $-(\gamma_{SL} - \gamma_{S0})$. The value of γ_{LV} was obtained from a standard simulation system with a planer liquid-vapor interface.[20,27] The interfacial tensions $-(\gamma_{SL} - \gamma_{S0})$ and $-(\gamma_{SV} - \gamma_{S0})$ showed the same dependence on η as the work of adhesion W_{SL} and W_{SV}, respectively, indicating that the interfacial tensions obtained by the mechanical and thermodynamic routes corresponded well for the present case of the flat and smooth fluid-wall interface on a densely-packed crystal surface. The good correspondence between $-(\gamma_{SL} - \gamma_{S0})$ and W_{SL} also indicated that these two calculated by two routes were differed exactly by γ_{LV}. Note that this correspondence was also because the Laplace pressure in the droplet was comparatively small so that the pressure dependence of γ_{SL} was negligibly small. In addition, for wettable cases of $\eta > 0.4$, $-(\gamma_{SV} - \gamma_{S0})$ or W_{SV} had a non-negligible value, indicating that the solid-vapor interfacial tension should be considered to properly estimate the contact angle.
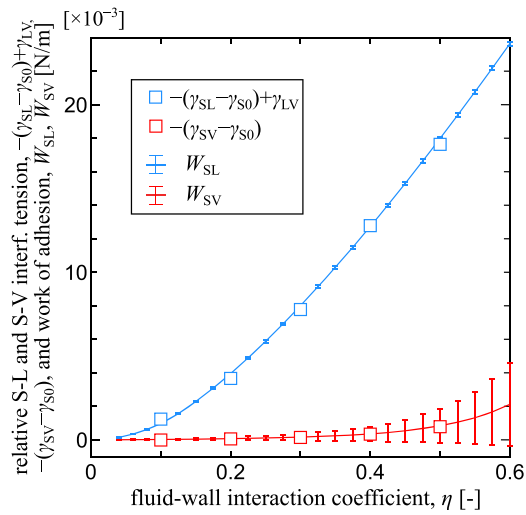
FIG. 7. Comparison between relative interfacial tensions obtained from the mechanical route and work of adhesion for flat SL and SV interfaces obtained by the DS method as a thermodynamic route. Considering the difference of the definitions, relative interfacial tensions $\gamma_{SL} - \gamma_{S0}$ and $\gamma_{SV} - \gamma_{S0}$ are shown as $-(\gamma_{SL} - \gamma_{S0}) + \gamma_{LV}$ and $-(\gamma_{SV} - \gamma_{S0})$, respectively, where $\gamma_{LV} = 11.3 \times 10^{-3}$ N/m is added to $-(\gamma_{SL} - \gamma_{S0})$. The value of γ_{LV} was obtained from a standard simulation system with a planer liquid-vapor interface.[20,27] The error bars were obtained from the standard deviation.

Figure 8 shows the comparison among three contact angles (1) estimated by

$$\cos\theta = \frac{(\gamma_{SV} - \gamma_{S0}) - (\gamma_{SL} - \gamma_{S0})}{\gamma_{LV}}, \tag{37}$$

using the interfacial tensions γ_{SL} and γ_{SV} obtained through the mechanical route, (2) estimated by
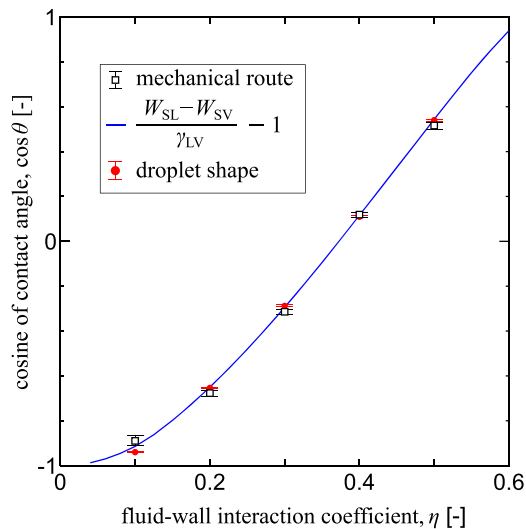

FIG. 8. Comparison between the apparent contact angle obtained from the droplet system and expected contact angle from the interfacial tensions obtained through mechanical and thermodynamic routes.

$$\cos\theta = \frac{W_{SL} - W_{SV}}{\gamma_{LV}} - 1, \tag{38}$$

using the SL and SV works of adhesion W_{SL} and W_{SV}, respectively, and (3) directly measured from the apparent shape in the droplet system in which the angle was defined by the angle between the least-squares fitting circle to a density contour line of $\rho = 400$ kg/m^3 for $z > z_{AL}$ and the plane of $z = z_{SA}$ at the intersection, as indicated in Fig. 6.[20] Note that we could give a strict choice of the density value for the contour as well,[44] but the result was not sensitive to the choice because the LV-interface was relatively thin. The value of $\gamma_{LV} = 11.3 \times 10^3$ N/m[20] was also used as well. It was shown that the three contact angles agreed quantitatively well for the present case. The correspondence between the mechanical route and apparent contact angle was achieved because the solid-fluid interface was properly given, which was used for the range of the lateral fluid stress integration. At present, we have not identified a clear reason for the difference between the mechanical route and droplet shape for a lower η of 0.1 yet, and further analysis on the following possible causes is needed: (1) the rather arbitrary choice of the density value of $\rho = 400$ kg/m^3 for the shape fitting, (2) spatial resolution of the stress calculation which directly affects the stress integral in Eq. (17), and (3) assumption of γ_{LV} to be constant irrespective of the curvature.

E. Discussion

The surface tensions calculated from fluid stress tensors were well converged in the present work for the LJ system on a rather hard, flat, and smooth solid crystal surface. A question arises whether this may or may not be the case for molecular solids because the residual stress and internal dynamics in the solid usually cause problem.[45,46] The effects of the change of solid volume were explicitly taken into account in the TI scheme Kanduč and Netz.[31] For the mechanical path, since Eq. (15) is exact, it follows without assuming the zero-external force condition in Eq. (23) and using Eq. (33) that

$$\int_{z_{bot}}^{z_{AL}} \tau_{xx}(x_{CV}, z)dz - \int_{z_{bot}}^{z_{AL}} \tau_{xx}(x_{LC}, z)dz - \gamma_{LV}\cos\theta'$$
$$= -\iint_V f_x^{ext}(x, z)dV, \tag{39}$$

where V denotes the range of $x_{LC} \le x \le x_{CV}$ and $z_{bot} \le z \le z_{AL}$, as long as we take the height of the bottom face of the control volume z_{bot} well below the solid-fluid interface so that

$$\int_{x_{LC}}^{x_{CV}} \tau_{zx}(x, z_{bot})dx = 0 \tag{40}$$

is satisfied. Then, the effects of the residual stress and the internal dynamics as well as the surface deformation[45,46] can be embedded into the external force in Eq. (39). We do not expect difficulties with the convergence of the fluid stress integrals and volume integral of the external force in Eq. (39). Ambiguity could arise when we transform the fluid stress integrals in the LHS of Eq. (39) by Eqs. (27) and (28), in which the

bottom position must be defined for $\tau_{\text{bulk}} \neq 0$. We think that the definition becomes difficult for relatively soft molecular solids, where we would have to introduce different z_{SL} and z_{SV} due to the solid deformation, for instance.

Regarding the mechanical path, we have only examined the force balance tangential to the surface, but it is also technically trivial to deal with the surface-normal force balance using the present fluid stress. Further analysis on this surface normal force would give valuable information about $\gamma_{\text{LV}} \sin\theta$ which is related to the disjoining pressure.[45–47]

With respect to the comparison between mechanical and thermodynamic paths, since the SL-DS simulations were performed in the NPT ensemble, the resulting W_{SL} was the work of adhesion at the prescribed pressure at 1 MPa rather than at the coexistence condition. On the other hand, the SV-DS simulations were under coexistence condition with the particle bath. These two mean that both the resulting W_{SL} and W_{SV} are under conditions slightly different from the coexistence condition in the droplet simulations. However, W_{SL} was not sensitive to the pressure even within the present range of Laplace pressure of up to a few MPa, as shown in Fig. 3. For W_{SV}, its absolute value was small compared to W_{SL}, and the effect of vapor pressure on the evaluation of Young's equation was considered to be negligible. These are because we have used a relatively hard solid crystal surface without polarity in the present study. Indeed, non-negligible effect of vapor pressure was shown by Kanduč and Netz[31] for a system with water on a polar solid surface. Related to these points, the solid-vacuum interfacial tension γ_{s0} is included in Eqs. (11) and (13), and the pressure effect on γ_{s0} should be included for a system with a soft solid subject to considerable deformation due to pressure; however, this is not the case for the present system.

Finally, a further analysis on the system size dependence would give new insight with regard to the finite-size scaling analysis on the wetting transition.[18] Although we did not test the size dependence of the solid-related interfacial tensions, the curvature dependence of the liquid-vapor interfacial tension γ_{LV} was small for the size range of the present droplets.[20,44]

IV. CONCLUSIONS

We carried out MD simulations of a cylindrical Lennard-Jones droplet on a flat and smooth solid surface. We examined in detail the surface-lateral force balance on a control volume set around the contact line and theoretically connected the fluid stress integral along each face of the control volume with the corresponding interfacial tension. Through this connection, we showed that Young's equation was only applicable to a system in which the net lateral force exerted on the fluid molecules from the solid surface was zero around the contact line. This condition would be easily violated for systems with realistic molecular fluids and/or the solid surface terminated with functional groups. Furthermore, we showed that the solid-liquid and solid-vapor interfacial tensions relative to the vacuum-solid one obtained by mechanical and thermodynamic approaches through an

extended Bakker's equation and DS method, respectively, were in good agreement. In addition, the contact angle predicted by Young's equation with these interfacial tensions corresponded well to the apparent droplet contact angle determined by using the previously defined position of the solid-fluid interface plane; however, our theoretical derivation indicated that this correspondence was achieved because the zero-lateral force condition was satisfied in the present system with a flat and smooth solid surface. These results indicated that the pinning force density should be additionally included in Young's equation to predict the contact angle.

APPENDIX A: LOWER LIMIT OF THE FLUID STRESS INTEGRATION AT THE SOLID-FLUID INTERFACE

When Eq. (23) is satisfied, Eq. (29) holds even if the lower limit of the integral for the 1st and 2nd terms of LHS is taken at an arbitrary position below z_{SA} because $\tau_{xx}(x, z) = 0$ for $z < z_{\text{SA}}$. Let $z'_{\text{SA}}(<z_{\text{SA}})$ be the arbitrary lower limit, it follows for Eq. (29) that

$$\int_{z'_{\text{SA}}}^{z_{\text{AL}}} \left(\tau_{xx}(x_{\text{CV}}, z) - \tau_{\text{V}}^{\text{bulk}}\right)dz - \int_{z'_{\text{SA}}}^{z_{\text{AL}}} \left(\tau_{xx}(x_{\text{LC}}, z) - \tau_{\text{L}}^{\text{bulk}}\right)dz$$
$$+ (z_{\text{AL}} - z'_{\text{SA}})(p_{\text{int}} - p_{\text{ext}}) - \gamma_{\text{LV}}\cos\theta' = 0. \tag{A1}$$

Considering that $\tau_{xx}(x_{\text{CV}}, z) = 0$ for $z < z_{\text{SA}}$, the 1st term of the LHS of Eq. (A1) is rewritten as

$$\int_{z'_{\text{SA}}}^{z_{\text{AL}}} \left(\tau_{xx}(x_{\text{CV}}, z) - \tau_{\text{V}}^{\text{bulk}}\right)dz$$
$$= \int_{z'_{\text{SA}}}^{z_{\text{SA}}} \left(0 - \tau_{\text{V}}^{\text{bulk}}\right)dz + \int_{z_{\text{SA}}}^{z_{\text{AL}}} \left(\tau_{xx}(x_{\text{CV}}, z) - \tau_{\text{V}}^{\text{bulk}}\right)dz$$
$$= -(z_{\text{SA}} - z'_{\text{SA}})\tau_{\text{V}}^{\text{bulk}} + \int_{z_{\text{SA}}}^{z_{\text{AL}}} \left(\tau_{xx}(x_{\text{CV}}, z) - \tau_{\text{V}}^{\text{bulk}}\right)dz. \tag{A2}$$

The 2nd term of the LHS of Eq. (A1) is rewritten as

$$\int_{z'_{\text{SA}}}^{z_{\text{AL}}} \left(\tau_{xx}(x_{\text{LC}}, z) - \tau_{\text{L}}^{\text{bulk}}\right)dz = -(z_{\text{SA}} - z'_{\text{SA}})\tau_{\text{L}}^{\text{bulk}}$$
$$+ \int_{z_{\text{SA}}}^{z_{\text{AL}}} \left(\tau_{xx}(x_{\text{LC}}, z) - \tau_{\text{L}}^{\text{bulk}}\right)dz. \tag{A3}$$

By substituting Eqs. (A2) and (A3) into Eq. (A1) as well as using $\tau_V^{\text{bulk}} = -p_{\text{ext}}$ and $\tau_L^{\text{bulk}} = -p_{\text{int}}$, Eq. (34) is recovered.

APPENDIX B: FORCE BALANCE FOR FLAT LV INTERFACE

Suppose a rectangular control volume around a contact line on a flat and smooth surface in Fig. 9 with a semi-infinite flat LV interface, which is similar to the control volume in Fig. 2 with a curved LV interface. Because the LV interface is semi-infinite in this case, we can take the position of the horizontal top face rather arbitrary as long as it is sufficiently away from the adsorption layers because the angle between the LV interface and top face is constant and independent of the position. Similarly, the position of the left face may be set arbitrary as long as it is sufficiently away from the contact line. Hence, let z_{top}, x_L, and x_V be the vertical position of the top face, horizontal positions of the left and right faces, respectively. Then, considering Eq. (22), it follows for the horizontal force balance on this control volume that

$$\int_{z_{\text{SA}}}^{z_{\text{top}}} \tau_{xx}(x_V, z)dz - \int_{z_{\text{SA}}}^{z_{\text{top}}} \tau_{xx}(x_L, z)dz + \int_{x_L}^{x_V} \tau_{zx}(x, z_{\text{top}})dx = 0. \tag{B1}$$

By taking the x' and z' axes in tangential and normal directions, respectively, as in Fig. 9, and considering that $\tau_{z'x'} = 0$ is satisfied between $(x, z) = (x_L, z_{\text{top}})$ and (x_V, z_{top}) because of the symmetry of the fluid stress in the z'-direction, the shear stress τ_{zx} in the 3rd term of the LHS of Eq. (B1) is rewritten as

$$\tau_{zx} = \cos\theta \sin\theta (\tau_{z'z'} - \tau_{x'x'}), \tag{B2}$$

where θ is the angle from the x- to x'-direction in the clockwise direction, which is equal to the angle from the SL interface to the LV-interface crossing at the apparent contact line
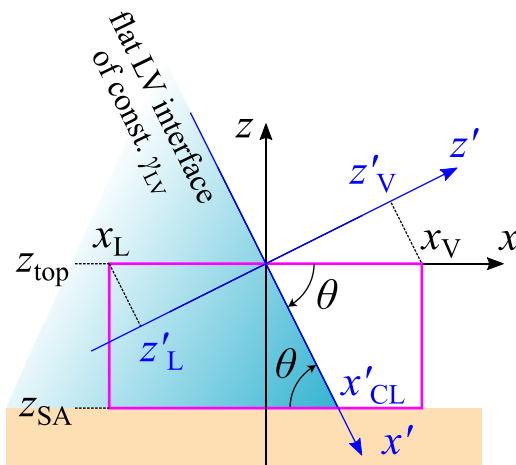
at $x' = x'_{\text{CL}}$ shown in Fig. 9. Thus, it follows for the 3rd term of the LHS of Eq. (B1) that

$$\int_{x_L}^{x_V} \tau_{zx}(x, z_{\text{top}})dx = \cos\theta \int_{x_L}^{x_R} [\tau_{z'z'}(x, z_{\text{top}}) - \tau_{x'x'}(x, z_{\text{top}})]\sin\theta dx$$
$$= \cos\theta \int_{z'_L}^{z'_R} [\tau_{z'z'}(x, z_{\text{top}}) - \tau_{x'x'}(x, z_{\text{top}})]dz', \tag{B3}$$

where z'_L and z'_V are the z'-coordinate of the top-left and top-right points of the control volume, respectively. Considering that $\tau_{z'z'}$ and $\tau_{x'x'}$ are a unique function of z'-coordinate away from the contact line with $x' \ll x'_{\text{CL}}$, the right-most hand side of Eq. (B3) is rewritten as

$$\cos\theta \int_{z'_L}^{z'_R} [\tau_{z'z'}(x, z_{\text{top}}) - \tau_{x'x'}(x, z_{\text{top}})]dz'$$
$$= \cos\theta \int_{z'_L}^{z'_R} [\tau_{z'z'}(z') - \tau_{x'x'}(z')]dz' \bigg|_{x' \ll x'_{\text{CL}}}$$
$$= -\gamma_{\text{LV}}\cos\theta, \tag{B4}$$

where Bakker's equation (26) is adopted for the second equality. Finally, by once removing the bulk isotropic fluid stress values τ^{bulk} as in Eq. (34), which is identical in the liquid and vapor bulks in the present system without Laplace pressure, it follows for Eq. (B1) that

$$\int_{z_{\text{SA}}}^{z_{\text{top}}} \left(\tau_{xx}(x_V, z) - \tau^{\text{bulk}}\right)dz - \int_{z_{\text{SA}}}^{z_{\text{top}}} \left(\tau_{xx}(x_L, z) - \tau^{\text{bulk}}\right)dz$$
$$- \gamma_{\text{LV}}\cos\theta = 0. \tag{B5}$$

By substituting the 1st and 2nd terms with the left-most hand sides of Eqs. (28) and (27), respectively, Young's equation (1) is derived. Note that in comparison with Eq. (34) for a hemi-cylindrical droplet system with $\theta \neq \theta'$, Eq. (B5) without the Laplace pressure is not sensitive to the definition of z_{SA}.

REFERENCES

[1] P.-G. de Gennes, Rev. Mod. Phys. **57**, 827 (1985).
[2] J. S. Rowlinson and B. Widom, *Molecular Theory of Capillarity* (Dover, 1982).
[3] S. Ono and S. Kondo, "Molecular theory of surface tension in liquids," in *Encyclopedia of Physics, Handbuch der Physik* (Springer, 1960), pp. 134–280.
[4] T. Young, Philos. Trans. R. Soc. London **95**, 65 (1805).
[5] L. Gao and T. J. McCarthy, Langmuir **25**, 14105 (2009).
[6] L. R. White, J. Chem. Soc., Faraday Trans. 1 **73**, 390 (1977).
[7] L. Boruvka and A. W. Neumann, J. Chem. Phys. **66**, 5464 (1977).
[8] A. Marmur, J. Colloid Interface Sci. **186**, 462 (1997).
[9] M. N. Popescu, G. Oshanin, S. Dietrich, and A. M. Cazabat, J. Phys.: Condens. Matter **24**, 243102 (2012).
[10] V. K. Kumikov and K. B. Khokonov, J. Appl. Phys. **54**, 1346 (1983).
[11] W. R. Tyson and W. A. Miller, Surf. Sci. **62**, 267 (1977).
[12] J. G. Kirkwood and F. P. Buff, J. Chem. Phys. **17**, 338 (1949).
[13] M. J. P. Nijmeijer and J. M. J. van Leeuwen, J. Phys. A: Math. Gen. **23**, 4211 (1990).
[14] M. J. P. Nijmeijer, C. Bruin, A. F. Bakker, and J. M. J. van Leeuwen, Phys. Rev. A **42**, 6052 (1990).
[15] J. Z. Tang and J. G. Harris, J. Chem. Phys. **103**, 8201 (1995).
[16] P. van Remoortere, J. E. Mertz, L. E. Scriven, and H. T. Davis, J. Chem. Phys. **110**, 2621 (1999).

FIG. 9. Example system for the analysis of horizontal force balance exerted on a rectangular control volume shown in magenta set around the contact line of the flat LV interface.

[17] T. Ingebrigtsen and S. Toxvaerd, J. Phys. Chem. C **111**, 8518 (2007).

[18] S. K. Das and K. Binder, Europhys. Lett. **92**, 26006 (2010).

[19] D. Seveno, T. D. Blake, and J. De Coninck, Phys. Rev. Lett. **111**, 096101 (2013).

[20] S. Nishida, D. Surblys, Y. Yamaguchi, K. Kuroda, M. Kagawa, T. Nakajima, and H. Fujimura, J. Chem. Phys. **140**, 074707 (2014).

[21] G. J. Gloor, G. Jackson, F. J. Blas, and E. De Miguel, J. Chem. Phys. **123**, 134703 (2005).

[22] G. V. Lau, I. J. Ford, P. A. Hunt, E. A. Müller, and G. Jackson, J. Chem. Phys. **142**, 114701 (2015).

[23] E. M. Grzelak and J. R. Errington, J. Chem. Phys. **128**, 014710 (2008).

[24] V. Kumar and J. R. Errington, Phys. Procedia **53**, 44 (2014).

[25] F. Leroy, D. J. V. A. Dos Santos, and F. Müller-Plathe, Macromol. Rapid Commun. **30**, 864 (2009).

[26] F. Leroy and F. Müller-Plathe, J. Chem. Phys. **133**, 044110 (2010).

[27] D. Surblys, Y. Yamaguchi, K. Kuroda, M. Kagawa, T. Nakajima, and H. Fujimura, J. Chem. Phys. **140**, 034505 (2014).

[28] F. Leroy and F. Müller-Plathe, Langmuir **31**, 8335 (2015).

[29] V. R. Ardham, G. Deichmann, N. F. van der Vegt, and F. Leroy, J. Chem. Phys. **143**, 243135 (2015).

[30] D. Surblys, F. Leroy, Y. Yamaguchi, and F. Müller-Plathe, J. Chem. Phys. **148**, 134707 (2018).

[31] M. Kanduč, J. Chem. Phys. **147**, 174701 (2017).

[32] H. Jiang, F. Müller-Plathe, and A. Z. Panagiotopoulos, J. Chem. Phys. **147**, 084708 (2017).

[33] S. Ravipati, B. Aymard, S. Kalliadasis, and A. Galindo, J. Chem. Phys. **148**, 164704 (2018).

[34] G. Bakker, *Kapillarität und Oberflächenspannung* (Wien-Harms, 1928), Vol. 6.

[35] S. M. Thompson, K. E. Gubbins, J. P. R. B. Walton, R. A. R. Chantry, and J. S. Rowlinson, J. Chem. Phys. **81**, 530 (1984).

[36] D. Surblys, Y. Yamaguchi, K. Kuroda, T. Nakajima, and H. Fujimura, J. Chem. Phys. **135**, 014703 (2011).

[37] J. H. Weijs, A. Marchand, B. Andreotti, D. Lohse, and J. H. Snoeijer, Phys. Fluids **23**, 022001 (2011).

[38] J. Blömer and A. E. Beylich, Surf. Sci. **423**, 127 (1999).

[39] D. Evans and G. Morriss, *Statistical Mechanics of Nonequilibrium Liquids*, 2nd ed. (Cambridge University Press, 2008), pp. 107–111.

[40] D. Schofield and J. R. Henderson, Proc. R. Soc. London, Ser. A **379**, 231 (1982).

[41] J. S. Rowlinson, Pure Appl. Chem. **65**, 873 (1993).

[42] D. Frenkel and B. Smit, *Understanding Molecular Simulation: From Algorithms to Applications* (Academic Press, 1996), pp. 152–156.

[43] A. Marchand, J. H. Weijs, J. H. Snoeijer, and B. Andreotti, Am. J. Phys. **79**, 999 (2012).

[44] H. Yaguchi, T. Yano, and S. Fujikawa, J. Fluid Sci. Technol. **5**, 180 (2010).

[45] L. R. White, J. Colloid Interface Sci. **258**, 82 (2003).

[46] S. Das, A. Marchand, B. Andreotti, and J. H. Snoeijer, Phys. Fluids **23**, 072006 (2011).

[47] J. Henderson, Phys. Rev. E **69**, 061613 (2011).